

Compound Fault Diagnosis for Train Transmission Systems Using Deep Learning with Fourier-enhanced Representation

Jonathan Adam Rico
Engineering Product Development
SUTD
Institute for Infocomm Research
*A*STAR*
Singapore
jonathanadam_rico@mymail.sutd.edu.sg

Nagarajan Raghavan*
Engineering Product Development
SUTD
Singapore
nagarajan@sutd.edu.sg

*Corresponding author

Senthilnath Jayavelu
Institute for Infocomm Research
*A*STAR*
Singapore
j_senthilnath@i2r.a-star.edu.sg

Abstract—Fault diagnosis prevents train disruptions by ensuring the stability and reliability of their transmission systems. Data-driven fault diagnosis models have several advantages over traditional methods in terms of dealing with non-linearity, adaptability, scalability, and automation. However, existing data-driven models are trained on separate transmission components and only consider single faults due to the limitations of existing datasets. These models will perform worse in scenarios where components operate with each other at the same time, affecting each component's vibration signals. To address some of these challenges, we propose a frequency domain representation and a 1-dimensional convolutional neural network for compound fault diagnosis and applied it on the PHM Beijing 2024 dataset, which includes 21 sensor channels, 17 single faults, and 42 compound faults from 4 interacting components, that is, motor, gearbox, left axle box, and right axle box. Our proposed model achieved 97.67% and 93.93% accuracies on the test set with 17 single faults and on the test set with 42 compound faults, respectively.

Index Terms—Train fault diagnosis, Fourier transform, Convolutional neural network, Supervised autoencoder

I. INTRODUCTION

Fault diagnosis plays a crucial role in maintaining the stability and reliability of transmission components, helping to prevent disruptions in train operations. Identifying and addressing faults early ensures that trains can run smoothly without unexpected interruptions, ultimately enhancing the overall safety and efficiency of the transportation system. Existing fault diagnosis models are trained on datasets that have motor current and vibration data on individual components [1]. In practice, train transmission systems are made up of several components such as motor, gearbox, and axle boxes that interact with each other. Moreover, multiple faults of the same or different components may occur at the same time.

Fault diagnosis using motor current and vibration signals is a time series classification task. Thus, time series signal processing methods, techniques, and representations can be applied such as spectral analysis [2], statistical and probabilistic analysis [3], blind deconvolution [4], fast Fourier transform

(FFT) [5], short-time Fourier transform (STFT) [6], and wavelet transform (WT) [7]. The WT representation provides both spectral and temporal features, but given a static dataset, FFT representation can be enough. The FFT representation is widely utilized in different fault diagnosis fields [5] [8] due to its ability to detect fault frequencies, identify multiple faults in a single analysis, and offer computational efficiency.

Several machine learning models were developed for fault diagnosis, such as the Support Vector Machine (SVM) [9], K-Nearest Neighbors (KNN) [10], Random Forest (RF) [11], and Extreme Learning Machine (ELM) [12]. However, such models rely on feature extraction techniques to transform the input signals into structured tabular data. In contrast to machine learning models, deep learning models do not require feature extraction from time series vibration signals into structured tabular features. Some of the most commonly used deep learning models for fault diagnosis include recurrent architecture [13], CNN [14], graph-based models [1], autoencoder-based architectures [15], and transformer-based architectures [16]. A summary table of the commonly used methods for bearing fault diagnosis is shown in Table I.

The key contributions of our work are as follows:

- We developed a fault diagnosis model that can detect compound faults in a train transmission system where the vibration measurements of each component affect the vibration measurements of adjacent component.
- By taking the amplitude spectrum of the raw signals with FFT and efficiently identifying the speed working condition for data normalization, we enhance the feature representation of the motor current and vibration signals.
- Using 1DCNN feature extraction further improves the fault diagnosis due to the translational invariance of CNN making the deep learning model robust to frequency shifts.

TABLE I
EXISTING METHODS FOR BEARING FAULT DIAGNOSIS.

Method	Algorithm	Related Literature
Traditional/ Feature Representation	Spectral analysis	[2]
	FFT	[5]
	WT	[7]
	Blind Deconvolution	[4]
	Statistical	[3]
Machine Learning	STFT	[6]
	SVM	[9]
	KNN	[10]
	RF	[11]
Deep Learning	ELM	[12]
	RNN	[13] [23]
	CNN	[1] [14] [19] [20] [23] [29]
	Autoencoder	[15]
	GNN	[1]
	Transformer	[16]

II. RELATED WORKS

Table II shows the description of the existing bearing fault diagnosis datasets used in the literature. Datasets for bearing fault diagnosis, such as the Case Western Research University (CWRU) dataset [17], Paderborn University bearing dataset [18], Vishwakarma Institute of Technology (VIT) College motor bearing dataset [19], High-speed train (HST) wheelset bearing dataset [20], Hanoi University of Science and Technology (HUST) bearing dataset [21], and the HST axle box bearing dataset [22] do not consider the interactions between components. Moreover, these datasets only tackle single faults in bearings. On the other hand, Prognostics and Health Management (PHM) Beijing 2024 dataset [1] consists of compound faults and considers vibrational interactions between transmission components. Fig. 1 shows the experimental platform of the train bogie used to collect sensor data from the motor, gearbox, left axle box, and right axle box.

Numerous fault diagnosis models were proposed that utilize CNN architecture, including an adaptive multiscale fully convolutional network (AMFCN) [14], self-supervised CNN (SSCNN) [20], 1DCNN-LSTM [23], end-to-end CNN [24], and multitask 1DCNN [25]. However, these models do not have data representation and directly input the raw signals into their CNN architectures. In addition, they develop fault diagnosis models for individual components and only tackle single faults. Recent studies in fault diagnosis incorporated feature representations in their deep learning models such as discrete wavelet transform (DWT) in self-paced CNN [22], CNN-based model [26], deep belief network (DBN) [27]; continuous wavelet transform (CWT) in convolution feature-based RNN (CFRNN) [13], CWT-CNN [19], CNN-LSTM [28]; STFT representation in [15] proposed hybrid classification Autoencoder (HCAE); and FFT in transformer-based model [16], and 1DCNN [29]. However, these models were developed for fault diagnosis of individual components and only considering single faults. On the other hand, Ding et al. [1] proposed a graph-based compound fault diagnosis model for multiple component system. However, it did not use any preprocessing and feature representation. In our work, we have both feature

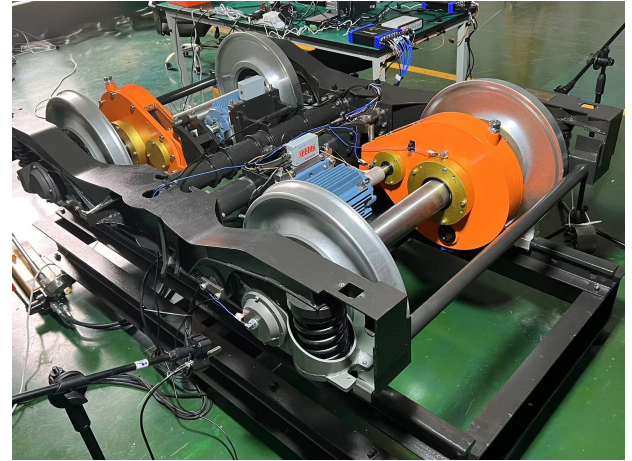


Fig. 1. Photo [1] of the experimental platform of the train bogie used in the PHM Beijing 2024 dataset.

representation and fault diagnosis on multiple components with compound faults.

III. METHODOLOGY

In this section, we discuss the theoretical preliminaries for feature representation, data preprocessing including feature selection and normalization by speed working conditions, and deep learning architecture for feature extraction and classification.

A. Preliminaries

1) *Fourier Transform*: The digitalized form of the Fourier transform is called the discrete Fourier transform (DFT). Given a raw signal $x^{(c)}[n]$ from channel c , data points N , the DFT is defined as,

$$X^{(c)}[k] = \sum_{n=0}^{N-1} x^{(c)}[n] e^{-j2\pi kn/N} \quad (1)$$

for $k = 0, 1, \dots, N-1$.

The calculation of DFT can be sped up by considering its even and odd symmetries, this algorithm, called Fast Fourier Transform (FFT) [30], is given by $X^{(c)}[k] = X_{even}^{(c)}[k] + X_{odd}^{(c)}[k]$, where,

$$X_{even}^{(c)}[k] = \sum_{m=0}^{M-1} x^{(c)}[2m] e^{-j2\pi km/N} \quad (2)$$

$$X_{odd}^{(c)}[k] = \sum_{m=0}^{M-1} x^{(c)}[2m+1] e^{-j2\pi k(m+1)/N} \quad (3)$$

whereas $M = N/2$ and $m \in [0, M-1]$. Since the motor current and vibration signals are only real-valued, their FFTs are Hermitian symmetric. Thus, we only need to consider the real part of the magnitude spectrum for each channel c given by,

$$|X^{(c)}[k]| = \sqrt{[\Re(X^{(c)}[k])]^2} \quad (4)$$

TABLE II
DESCRIPTION OF BEARING FAULT DIAGNOSIS DATASETS AND THE LITERATURE THAT USED THE DATASETS FOR FAULT DIAGNOSIS.

Dataset	Date	Components	Fault Types	Related Literature
CWRU bearing dataset [17]	2009	Bearings in motor	9 single faults, 1 normal	[13] [14] [15] [19] [23] [24] [25] [26] [29]
Paderborn University bearing dataset [18]	2016	Bearings in rolling element	26 single faults, 6 normal	[14]
VIT College motor bearing dataset [19]	2021	Bearings in motor and gearbox	2 single faults, 1 normal	[19]
HST wheelset bearing dataset [20]	2022	Bearings in train axlebox	10 single faults, 1 normal	[26]
HUST bearing dataset [21]	2023	Bearings in rolling element	6 single faults, 1 normal	[28]
PHM Beijing dataset [1]	2024	Bearings in train motor, gearbox, and axle boxes	42 compound faults	[1]
HST axle box bearing dataset [22]	2025	Bearings in train axle box	8 single faults, 1 normal	[22]

In addition to the simplified complexity due to the reduced input size, $N/2$, this magnitude spectrum $|X[k]|$ has several properties that are beneficial for feature representation:

- *Time Invariance.* FT is invariant to shifts in the time domain such that the FT of the shifted signal is the FT of the original signal with the same phase shift.

$$\mathcal{F}(x[n]) = X[k] \Rightarrow \mathcal{F}(x[n - k]) = X[k]e^{-j2\pi kn/N} \quad (5)$$

- *Magnitude Invariance.* If the signal is multiplied by a complex exponential, the magnitude $|X[k]|$ of the Fourier transform remains the same. This only causes phase shift in the amplitude spectrum that a CNN can capture.

$$\mathcal{F}(x[n]) = X[k] \Rightarrow \mathcal{F}(x[n]e^{j\phi}) = X[k]e^{j\phi} \quad (6)$$

- *Linear Property.* The Fourier transform of a linear combination of signals is equivalent to the linear combination of their Fourier transforms.

$$\mathcal{F}(ax_1[n] + bx_2[n]) = a|X_1[k]| + b|X_2[k]| \quad (7)$$

This property implies that the signals in frequency domain are viable inputs to the neural network since the neural network tries to derive the linear and non-linear relationships between the signals that would discriminate for each classes.

2) *Convolutional Neural Network:* CNNs [31] have useful properties such as translational invariance, invariance to scaling if there is batch normalization, and invariance to local variations. The global average pooling averages the input feature map B to have the sequence length reduced equivalent to kernel size g given by,

$$G = \frac{1}{g} \sum_{i=0}^{g-1} B_i. \quad (8)$$

Batch normalization normalizes the values using the mean μ_P and variance σ_P^2 of the mini batch P with the trainable parameters γ and β pertaining to scaling and shifting respectively and a very small value ϵ to avoid division by zero.

$$B_i = \gamma \cdot \frac{P_i - \mu_P}{\sqrt{\sigma_P^2 + \epsilon}} + \beta \quad (9)$$

Maximum pooling with the kernel size p reduces the sequence length.

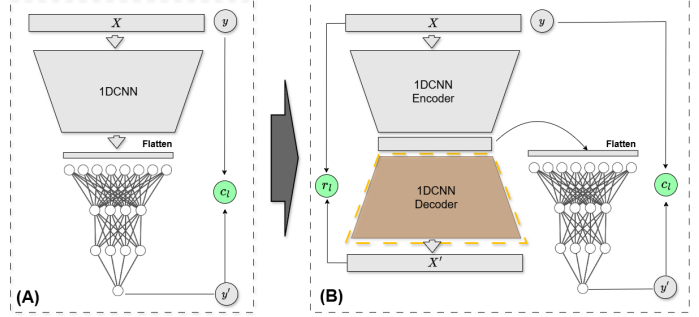


Fig. 2. Illustration of (A) 1DCNN architecture to (B) supervised autoencoder architecture. Where X and y are the input data and binary label; while X' and y' are the reconstructed input data and the predicted label.

$$P_i = \max(A_i, A_{i+1}, \dots, A_{i+p+1}) \quad (10)$$

Applying rectified linear unit (ReLU) activation function on the Conv1D output adds non-linearity to the model using,

$$A_i = \max(0, Y_i) \quad (11)$$

Given the input sequence x , the output Y of a one-dimensional convolution (Conv1D) of kernel size k with trainable weights w and bias b is,

$$Y_i = \sum_{j=1}^k w_j \cdot x_{i+j-1} + b. \quad (12)$$

3) *Supervised Autoencoder:* The Supervised Autoencoder architecture introduced by [32], is a regularizer similar to dropout layers, L1/L2 regularizer. The idea is that neural networks for supervised tasks can be further improved by incorporating an autoencoder architecture such that the loss function Eqn. (13) becomes a sum of classification loss (c_l) and reconstruction loss (r_l). The architecture of supervised autoencoder from a 1DCNN architecture is illustrated in Fig. 2. The authors of [32] claim that the classification performance is never harmed due to the added regularizer. The training tends to be more stable because the model also learns the underlying structure of the data due to the added reconstruction loss.

$$loss = c_l + r_l \quad (13)$$

TABLE III
DESCRIPTION OF SENSOR CHANNELS.

Channel	Component	Signal Type
CH1, CH2, CH3	Motor (drive end)	Tri-axial acceleration
CH4, CH5, CH6	Motor (fan end)	Tri-axial acceleration
CH7, CH8, CH9	Motor (cable)	Three-phase current
CH10, CH11, CH12	Gearbox (input axle)	Tri-axial acceleration
CH13, CH14, CH15	Gearbox (input axle)	Tri-axial acceleration
CH16, CH17, CH18	Axle box left (end cover)	Tri-axial acceleration
CH19, CH20, CH21	Axle box right (end cover)	Tri-axial acceleration

B. Data Preprocessing

The data preprocessing as illustrated in the initial steps of Fig. 3 involves feature selection, amplitude spectrum calculation of the selected raw signals and data normalization according to speed working condition which is derived from a simple speed identification task (SIT). There are a total of 21 channels which can all be inputs to the model. However, not all of those channels are relevant for each component fault diagnosis. For example, vibration signals in the left axle box may not be relevant for motor fault diagnosis, since they are not directly connected in physical structure. Thus, we performed feature (channel) selection based on the physical structure and connections of the components. The motor channels CH1-CH9, the gearbox channels CH10-CH15, the left axle box channels CH16-CH18, and the right axle box channels CH19-CH21 are described in Table III. The motor is connected to the gearbox, the left axle box is connected to the gearbox, and the right axle box is connected to the gearbox. Based on the selected raw input signals, we perform FFT to obtain the amplitude spectrum of each feature reducing the sequence length by half, from 64000 to 32000. The amplitude spectra are normalized according to the identified speed working condition, which is directly derived from the fundamental frequency, plus or minus some slip frequency, of its motor current signal CH7. The global minimum and maximum for each feature of the training set were stored for normalization of the validation and test sets. This benefits the training because neural network performs best when the input data are homogeneous and properly scaled. The normalized amplitude spectra are then fed into the 1DCNN model, which provides the binary classification of normal or anomaly for the particular fault type.

C. Deep Learning

The multiclass multilabel classification was divided into multiple binary classification tasks equivalent to the number of single faults, i.e. 17 binary classification models. The proposed FFT-1DCNN framework illustrated in Fig. 3 is patterned before the 1DCNN architecture of [1] which includes convolutional layers with rectified linear unit (ReLU) activation functions, max pooling layers, batch normalization, and a global averaging layer. The convolutional layers have a kernel size of 9, with padding 1, and stride 1. The max pooling layers have a kernel size of 4 and stride of 2. The classifier neural network architecture is [32, 16, 16] and a sigmoid.

We compared our proposed FFT-1DCNN with a similar framework with supervised autoencoder architecture. Figure 2

illustrates how it is implemented by adding a decoder network to the architecture so that the 1DCNN becomes the encoder. Then the flattened latent space also goes to the dense layer to obtain the binary classification.

IV. RESULTS AND DISCUSSION

A. Dataset Description

We use the publicly available train transmission dataset from the PHM-Beijing 2024 Data Challenge [1] which includes motor current and vibration signals of motor (M), gearbox (G), left axle (LA) box, and right axle (RA) box. Table III shows the description and specific location of the sensors that measure the signals, also referred to as channels, CH1-CH21. This dataset considers the vibrational interactions between the components. There are several challenges in the dataset:

- 1) **Multi-label classification.** Each sample can have normal or any combination of the other fault types of each component in Table IV. Such that for a sample, there are $(M)16 \times (G)256 \times (LA)16 \times (RA)2 = 131,072$ possible compound fault labels, calculated as the product of the combination of possible labels for each component, M, G, LA, and RA.
- 2) **Compound faults.** Each label in the subway train transmission dataset can be a combination of faulty and normal components, or only faulty components, or only normal components. For example, the motor is normal but the other components are faulty, in this case, the label is $M0_G1_LA2_RA1$. In such cases, the vibration signals might be affected by the fault of other components. Table V shows the 42 compound faults in this dataset.
- 3) **Varying and unknown working conditions** Signal data were collected from the subway train transmission system with 9 different working conditions, combination of different speed $v \in [20Hz, 40Hz, 60Hz]$ and lateral load $l \in [-10kN, 0kN, 10kN]$ working conditions. In addition, the dataset has information on the working conditions only for preliminary training and test sets. The rest of the samples do not have information on the working conditions.
- 4) **Imbalanced data.** The initial training set consists of 3 samples for each single fault type. For most fault types, when the data is split for binary classification, the normal to anomaly ratio is about 20:1 in most cases of the training set, as shown in Table VI.

B. Evaluation Metrics

The main performance metric for model evaluation is the Z metric which is a weighted combination of accuracy, precision, recall, and f1 score introduced in the PHM-Beijing 2024 Data Challenge. This metric provides a better evaluation than the commonly used metric, accuracy, which does not provide a clear indication if the data is highly imbalanced. In the discussions, we often refer to accuracy to compare with existing studies, since the Z metric was only introduced in 2024 for the PHM Data Challenge, 2024.icphm.org.

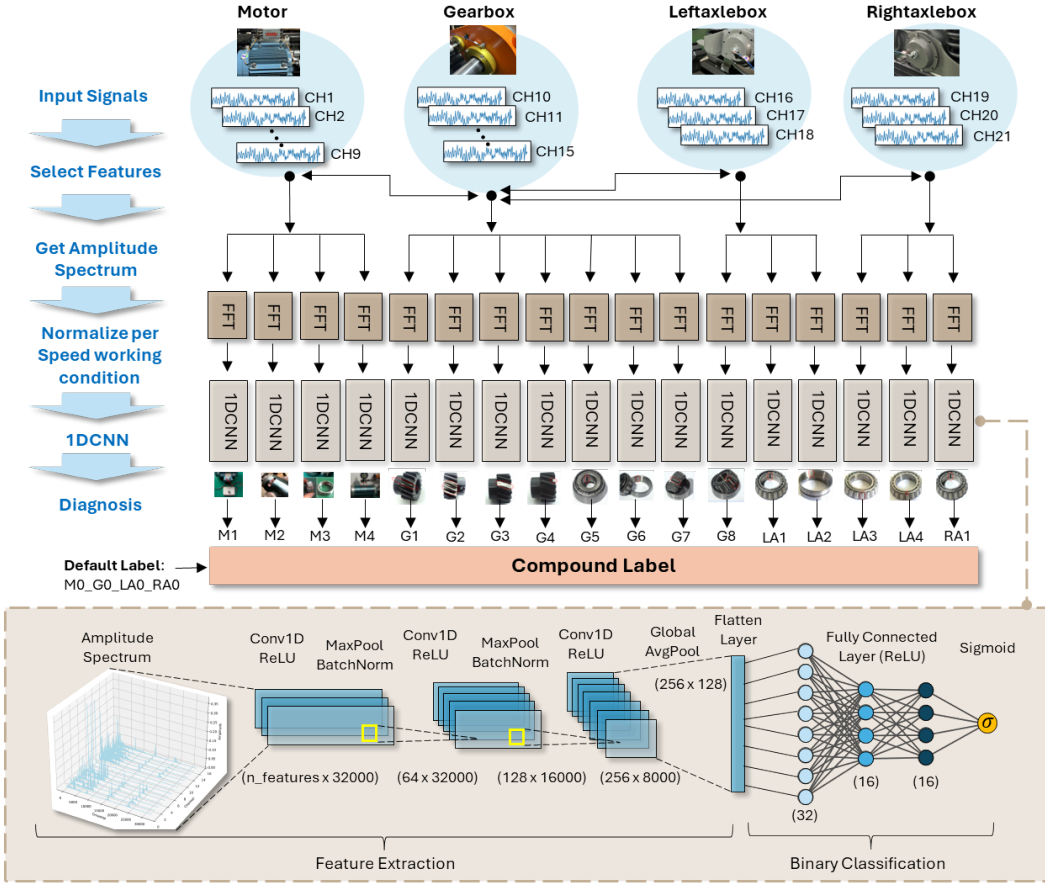


Fig. 3. Proposed compound fault diagnosis framework using FFT-1DCNN.

TABLE IV
DESCRIPTION OF FAULT TYPES.

Fault Code	Description
M0,G0,LA0,RA0	Normal component
M1	Motor - short circuit
M2	Motor - broken rotor bar
M3	Motor - bearing fault
M4	Motor - bowed rotor
G1	Gearbox - gear cracked tooth
G2	Gearbox - gear worn tooth
G3	Gearbox - gear missing tooth
G4	Gearbox - gear chipped tooth
G5	Gearbox - bearing inner race fault
G6	Gearbox - bearing outer race fault
G7	Gearbox - bearing rolling element fault
G8	Gearbox - bearing cage fault
LA1	Left Axle Box - bearing inner race fault
LA2	Left Axle Box - bearing outer race fault
LA3	Left Axle Box - bearing rolling element fault
LA4	Left Axle Box - bearing cage fault
RA1	Right Axle Box - bearing inner race fault

$$Z = 0.4(Acc) + 0.2(Prec) + 0.2(Rec) + 0.2(F1) \quad (14)$$

where,

$$Accuracy = \frac{TP + TN}{TP + TN + FP + FN} \quad (15)$$

$$Precision = \frac{TP}{TP + FP} \quad (16)$$

$$Recall = \frac{TP}{TP + FN} \quad (17)$$

$$F1 = 2 \times \frac{Precision \times Recall}{Precision + Recall} \quad (18)$$

Where TP, TN, FP, and FN are true positives, true negatives, false positives, and false negatives, respectively.

Moreover, we measured the model complexity by calculating the floating point operations per second (FLOPs) of each model, exclusive of the preprocessing steps, using Pytorch *ptflops* module. A higher FLOPs metric means that the model is more complex and has a longer run time.

C. Implementation Details

The numerical simulation was implemented using Python language and Pytorch deep learning library on a computer workstation with a NVIDIA 16 GB GPU GeForce RTX 4080

TABLE V

FOURTY TWO (42) COMPOUND LABELS OF PHM BEIJING 2024 DATASET AND WHETHER THEY ARE PRESENT IN TRAINING SET, PRELIMINARY TEST SET, AND FINAL TEST SET.

No.	Compound label	Train	Test		Fault	Train		Validation		Test	
			Prelim	Final		normal	anomaly	normal	anomaly	normal	anomaly
1	M0_G0_LA0_RA0		✓	✓	✓	815	75	211	21	222	30
2	M1_G0_LA0_RA0		✓	✓	✓	840	40	222	20	222	30
3	M2_G0_LA0_RA0		✓	✓	✓	840	40	222	20	228	26
4	M3_G0_LA0_RA0		✓	✓	✓	840	40	222	20	234	18
5	M4_G0_LA0_RA0		✓	✓	✓	840	40	222	20	240	12
6	M0_G1_LA0_RA0		✓	✓	✓	840	40	222	20	240	12
7	M0_G2_LA0_RA0		✓	✓	✓	835	45	221	21	210	42
8	M0_G3_LA0_RA0		✓	✓	✓	829	70	203	20	240	12
9	M0_G4_LA0_RA0		✓	✓	✓	829	70	203	20	198	54
10	M0_G5_LA0_RA0		✓	✓	✓	840	40	222	20	246	6
11	M0_G6_LA0_RA0		✓	✓	✓	840	40	222	20	246	6
12	M0_G7_LA0_RA0		✓	✓	✓	790	100	200	32	180	72
13	M0_G8_LA0_RA0		✓	✓	✓	838	70	194	20	210	42
14	M0_G0_LA1_RA0		✓	✓	✓	820	70	212	20	228	24
15	M0_G0_LA2_RA0		✓	✓	✓	838	70	194	20	228	24
16	M0_G0_LA3_RA0		✓	✓	✓	894	4	222	2	234	18
17	M0_G0_LA4_RA0		✓	✓	✓						
18	M0_G0_LA1+LA2+LA4_RA0		✓	✓							
19	M0_G4+G5_LA0_RA0		✓	✓							
20	M1_G0_LA1_RA1		✓	✓							
21	M0_G3_LA1_RA0		✓	✓							
22	M1_G0_LA1_RA0		✓	✓							
23	M4_G3_LA0_RA0		✓								
24	M0_G1+G5_LA0_RA0		✓								
25	M0_G0_LA2+LA3_RA0		✓								
26	M2_G0_LA1_RA0		✓								
27	M0_G0_LA2+LA4_RA0		✓								
28	M3_G3_LA0_RA0		✓								
29	M1_G5_LA0_RA0		✓								
30	M0_G2+G5_LA0_RA0		✓								
31	M0_G0_LA1+LA2_RA0		✓								
32	M1_G3_LA0_RA0		✓								
33	M3_G0_LA1_RA0		✓								
34	M3_G5_LA0_RA0		✓								
35	M0_G0_LA1_RA1		✓								
36	M0_G3+G5_LA0_RA0		✓								
37	M0_G0_LA1+LA2+LA3+LA4_RA0		✓								
38	M0_G0_LA1+LA2+LA3_RA0		✓								
39	M2_G5_LA0_RA0		✓								
40	M4_G5_LA0_RA0		✓								
41	M2_G3_LA0_RA0		✓								
42	M2_G0_LA1_RA1		✓								

SUPER. The training data were divided into 1-second nonoverlapping time slices, that is, 64000 timesteps per slice given that the sampling rate is 64 kHz. The training set is further divided into roughly 80% train and 20% validation sets depending on the fault type. Table VI shows the exact number of samples in each set after data splitting. There are two holdout test sets: the preliminary test set contains 102 samples of single faults, and the final test set contains 252 samples of both single and compound faults. The initial learning rates for training the 1DCNN is 0.0001 and 0.001 for the dense layer. The loss function is weighted binary cross entropy, *BCEwithLogitsLoss* and the gradient descent optimizer is the Adam optimizer. The models are trained for 100 iterations and a batch size of 32. The model weights of the epoch with the lowest validation loss were further used to test the model performance.

TABLE VI

DATA SPLITTING FOR TRAINING, VALIDATION, AND HOLD OUT FINAL TEST SET WITH COMPOUND FAULTS.

Fault	Train	Validation		Test		
	normal	anomaly	normal	anomaly	normal	anomaly
M1	815	75	211	21	222	30
M2	840	40	222	20	222	30
M3	840	40	222	20	228	26
M4	840	40	222	20	234	18
G1	840	40	222	20	240	12
G2	840	40	222	20	240	12
G3	835	45	221	21	210	42
G4	829	70	203	20	240	12
G5	829	70	203	20	198	54
G6	840	40	222	20	246	6
G7	840	40	222	20	246	6
G8	840	40	222	20	246	6
LA1	790	100	200	32	180	72
LA2	838	70	194	20	210	42
LA3	820	70	212	20	228	24
LA4	838	70	194	20	228	24
RA1	894	4	222	2	234	18

TABLE VII

ABLATION STUDY RESULTS.

Model	Accuracy		Z	
	Prelim	Final	Prelim	Final
Raw-1DCNN	0.7750	0.7617	0.6251	0.5972
FFT-1DCNN (all features)	0.9725	0.9263	0.9460	0.8614
FFT-1DCNN	0.9767	0.9393	0.9543	0.8866

D. Feature Representation

The feature space representation is visualized by plotting the parallel coordinates of the feature space output of the 1DCNN. Unlike t-SNE and UMAP which requires data reduction down to 2 or 3 dimensions, parallel coordinates plot can be visualized even with high dimension, e.g. 32 dimensions. From the latent space of size 256×128, we used the top 32 eigenvalues based on the principal component analysis (PCA). Fig. 4 shows parallel coordinate plots for 32 dimensions of different classification performance scenarios, such as fault M4 and fault G4. From this figure, we can show that the Fourier transform helps improve the feature representation of the data for fault diagnosis. For example, Fig. 4a shows several class separations in various coordinates. However, it is difficult to observe the separations from the rest of the plots, Fig. 4b-d.

E. Ablation Study

We performed ablation experiments on the proposed framework to examine the impact of each preprocessing step on the model performance. That is, by removing some of the steps or procedures in the algorithm, we analyze the effect of the performance. The first ablation experiment is performed by Raw-1DCNN without the Fourier transform preprocessing and the accuracy in the final test set was reduced by 17%. The second ablation experiment skipped the feature selection, FFT-1DCNN (all features), which slightly reduced the accuracy in the final test set by 1.3%. The results of the ablation experiments are summarized in Table VII.

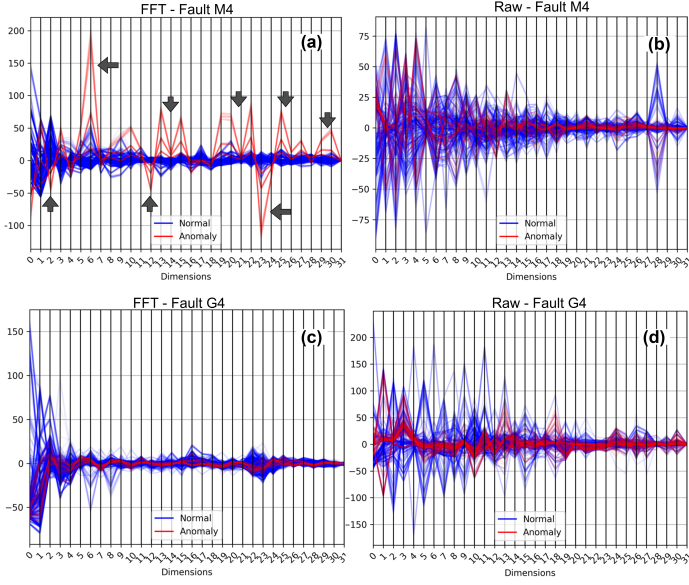


Fig. 4. Parallel coordinates plots of 1DCNN output feature space of the best case scenario (M4 fault) (a) with FFT representation, (b) using raw signals only, and the worst case scenario (G4 fault) (c) with FFT representation, (d) using raw signals only. The arrows in (a) indicate feature dimensions where there are clear disentanglement between classes. On the other hand, (b), (c), and (d) show that most feature dimensions are entangled.

F. Classification

Table VIII shows the comparison between the traditional unsupervised autoencoder, supervised convolutional autoencoder, and 1DCNN. It shows that the traditional unsupervised autoencoder, even with convolutional layers, does not perform well in this dataset's classification task. This is because the autoencoders prioritize learning the underlying structure by reconstructing the input data. On the other hand, by incorporating an additional regularizer into the FFT-1DCNN model using the supervised autoencoder architecture, its training stability and generalization improved by an accuracy of 93.97% on the final test set. The loss function is shown in Eqn. (19) which is a sum of binary cross entropy (BCE) and mean squared error (MSE). The constants λ_0 and λ_1 refer to the sensitivities of the BCE and MSE loss respectively. In this study, we have set $\lambda_0 = 1.0$ and $\lambda_1 = 0.1$ as the best performing sensitivity hyperparameters from the search space $\lambda_0 \in [0.01, 0.1, 1.0]$ and $\lambda_1 \in [0.01, 0.1, 1.0]$. Although the supervised autoencoder improved the performance, the improvement (+0.04% accuracy) is still comparable to the 1DCNN model and the supervised autoencoder has increased the model complexity by 6.8 MFLOPs from that of 1DCNN.

$$loss = \lambda_0 \text{ BCE} + \lambda_1 \text{ MSE} \quad (19)$$

Our model achieved 93.93% and 97.67% (binary class) accuracies and compared to the state-of-the-art, [1] achieved 94% to 98% diagnostic multiclass accuracies in a similar compound fault diagnosis dataset but different data settings. Fig. 5 shows the confusion matrices for selected fault types

TABLE VIII
SUMMARY OF PERFORMANCE ON BENCHMARK MODELS.

Model	Accuracy		Z		FLOPs
	Prelim	Final	Prelim	Final	
FFT-UnsupAE	0.5691	0.5480	0.4046	0.4075	11.9 M
FFT-SupConvAE	0.9757	0.9397	0.9526	0.8871	30.6 M
FFT-1DCNN	0.9767	0.9393	0.9543	0.8866	23.8 M

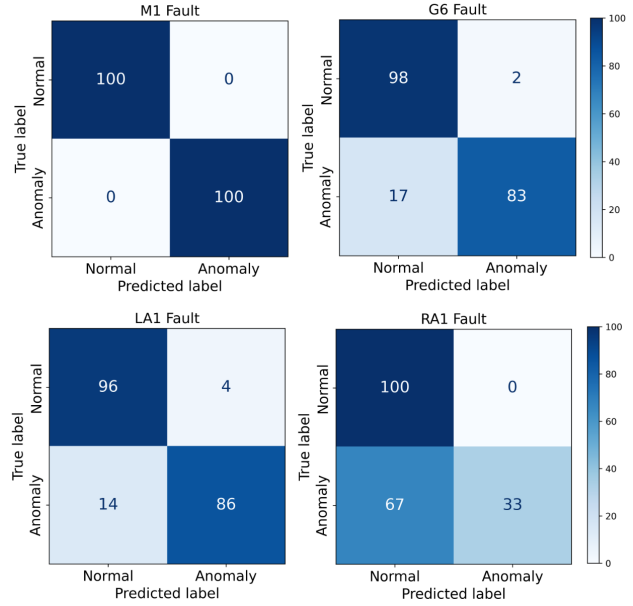


Fig. 5. Confusion matrices of selected faults on the final test set using FFT-1DCNN. The values are shown as percentages (%) due to data imbalance between classes.

M1, G6, LA1, and RA1. In terms of model complexity, [1] has 4.7 GFLOPs while our proposed model only has 23.8 MFLOPs.

V. CONCLUSION

In this paper, we investigate the advantages of using Fourier transform for time series data representation of vibration and motor current signals of subway train transmission system. We developed the FFT-1DCNN framework for subway train fault diagnosis using the recent PHM-Beijing 2024 dataset. We have shown that the frequency domain provides a better data representation as input for the fault diagnosis model utilizing a 1DCNN architecture, based on the model performance and parallel coordinates plots of the feature space. Our model has a comparable accuracy to that of FFT-SupervisedConvAE and [1] while having a lower model complexity in terms of FLOPs.

Our proposed framework has trade-offs in terms of model complexity and the number of models. The model's simple architecture of only 23.8 MFLOPs is also composed of several models (17 binary classifiers), which might be difficult to train and manage for industrial applications. The model also performs worse in gearbox faults, since all the other 3 components are directly connected to the gearbox, affecting its vibration signals. Moreover, the model does not perform well in the RA1 fault due to the small number of samples on this fault type. Lastly, the model assumes that the input data

have high sampling rates, e.g. 64kHz, and from multiple sensor channels attached close to each transmission component. This is because FFT suffers from aliasing and spectral leakage if the sampling rate is low and the model may not be able to distinguish between vibrations from different components if the sensor is only attached to the housing.

Our future work involves incorporating an evolvable CNN architecture [33] into our model framework for continual learning tasks. Such a model will be able to adapt to concept drifts, i.e. change of data distribution, while minimizing catastrophic forgetting. Furthermore, the study can be extended to include the enhanced FFT [34] which emphasizes the frequency peaks by minimizing the effects of spectral leakage.

DECLARATION OF COMPETING INTEREST

The authors declare that they have no known competing financial interests or personal relationships that could have appeared to influence the work reported in this paper.

DATA AVAILABILITY

The PHM Beijing 2024 dataset [1] is publicly available and can be accessed through their official website, 2024.icphm.org.

ACKNOWLEDGMENT

The first author acknowledges Singapore University of Technology and Design (SUTD) and the Ministry of Education, Singapore (MOE) for the Research Student Scholarship (RSS) and SUTD Ph.D. Fellowship for his doctoral studies from 2023-2026. The logistics of this research was also supported by the Research Surplus Grant No. RGSUR08 of Prof. Nagarajan Raghavan. The authors would also like to thank the Agency for Science, Technology, and Research (A*STAR) for providing computational resources for this study.

REFERENCES

- [1] A. Ding, Y. Qin, B. Guo, L. Jia, and X. Cheng, "Evolvable graph neural network for system-level incremental fault diagnosis of train transmission systems," *Mechanical Systems and Signal Processing*, 210, 2024.
- [2] J. Antoni, "Cyclic spectral analysis in practice." *Mechanical Systems and Signal Processing*, 21.2, 2007, pp.597-630.
- [3] A. Abid, M.T. Khan, and C.W. de Silva. "Layered and real-valued negative selection algorithm for fault detection." *IEEE Syst J*, 12(3), 2018, pp.2960-2969.
- [4] M. Buzzoni, J. Antoni, and G. d'Elia. "Blind deconvolution based on cyclostationarity maximization and its application to fault identification." *Journal of Sound and Vibration*, 2018 Oct 13, 432, pp.569-601.
- [5] H. Mahgoun, R.E. Bekka, and A. Felkaoui. "Gearbox fault detection using a new denoising method based on ensemble empirical mode decomposition and FFT." In: *4th International conference on integrity, reliability and failure (IRF2013)*, 2013, pp.1-11.
- [6] H. Geraei, E.A. Rodriguez, E. Majma, S. Habibi, D. Al-Ani. "A noise invariant method for bearing fault detection and diagnosis using adapted local binary pattern (ALBP) and short-time Fourier transform (STFT)." *IEEE Access*, 2024 Aug 5.
- [7] M.R.A.A Abad, A. Moosavian, and M. Khazaee. "Wavelet transform and least square support vector machine for mechanical fault detection of an alternator using vibration signal." *J Low Freq Noise Vib Active Control*, 35(1), 2016, pp.52-63.
- [8] L. Saribulut, A. Teke, and M. Tümay. "Fundamentals and literature review of Fourier transform in power quality issues." *Journal of Electrical and Electronics Engineering Research*. 5(1), 2013, pp.9-22.
- [9] X. Yan and M. Jia. "A novel optimized SVM classification algorithm with multi-domain feature and its application to fault diagnosis of rolling bearing." *Neurocomputing*, 313, 2018, pp.47-64.
- [10] A. Sharma, R. Jigyasu, L. Mathew, and S. Chatterji. "Bearing fault diagnosis using weighted k-nearest neighbor." *2nd Int. Conf. Trends Elec. Inf.*, 2018, pp.1132-1137.
- [11] H. Yan, H. Mu, X. Yi, Y. Yang, and G. Chen. "Fault Diagnosis of Rolling Bearing with Small Samples Based on Wavelet Packet Theory and Random Forest." *IEEE International Conference on Sensing, Diagnostics, Prognostics, and Control (SDPC)*, 2019 Aug 15, pp.305-310.
- [12] C. He, T. Wu, R. Gu, Z. Jin, R. Ma, and H. Qu. "Rolling bearing fault diagnosis based on composite multiscale permutation entropy and reverse cognitive fruit fly optimization algorithm-extreme learning machine." *Measurement*, 2021 Mar 1, 173, 108636.
- [13] D. Gao, Y. Zhu, Z. Ren, K. Yan, and W. Kang. "A novel weak fault diagnosis method for rolling bearings based on LSTM considering quasi-periodicity." *Knowledge-Based Systems*, 2021 Nov 14, 231, 107413.
- [14] F. Li, L. Wang, D. Wang, J. Wu, and H. Zhao. "An adaptive multiscale fully convolutional network for bearing fault diagnosis under noisy environments." *Measurement*, 2023 Jul 1, 216, 112993.
- [15] X. Wu, Y. Zhang, C. Cheng, and Z. Peng. "A hybrid classification autoencoder for semi-supervised fault diagnosis in rotating machinery." *Mechanical Systems and Signal Processing*, 2021 Feb 15, 149, 107327.
- [16] X. Luo, H. Wang, T. Han, and Y. Zhang. "FFT-Trans: Enhancing Robustness in Mechanical Fault Diagnosis With Fourier Transform-Based Transformer Under Noisy Conditions." *IEEE Transactions on Instrumentation and Measurement*, 2024 Mar 26.
- [17] K. Loparo. "Bearings Vibration Data Set, Cast Western Reverse University." From: <https://csegroups.case.edu/bearingdatacenter/home>, 1998, accessed on February 2025.
- [18] C. Lessmeier, J.K. Kimotho, D. Zimmer, W. Sextro, "Condition monitoring of bearing damage in electromechanical drive systems by using motor current signals of electric motors: A benchmark data set for data-driven classification," in: *Proc. Eur. Conf. Progn. Health Manag. Soc.*, 2016, pp.5-8.
- [19] Y.N. Aldeoes, P. Mahajan, and S.Y. Sondkar, "Advancements in Bearing Defect Diagnosis: Deep Learning-based Signal Processing and Real-time Fault Detection." *J Fail. Anal. Prev.*, 24(6), 2024, pp.2700-2713.
- [20] H. Wang, Z. Liu, Y. Ge, and D. Peng, "Self-supervised signal representation learning for machinery fault diagnosis under limited annotation data" *Knowledge-Based Systems*, 239, 2022, p.107978.
- [21] H.S. Hong and N. Thuan, "HUST bearing: a practical dataset for ball bearing fault diagnosis" *Mendeley Data*, 3, 2023.
- [22] K. Zhang, B. Wang, Q. Zheng, G. Ding, J. Ma, and B. Tang, "A novel fault diagnosis of high-speed train axle box bearings with adaptive curriculum self-paced learning under noisy labels." *Struct. Health Monit.*, 2025.
- [23] H. Pan, H. Xingxi, T. Sai, and M. Fanming. "An improved bearing fault diagnosis method using one-dimensional CNN and LSTM." *Journal of Mechanical Engineering/Strojniški Vestnik*, 64, 2018.
- [24] L.L. Kou, Y. Qin, X.J. Zhao, and X.A. Chen. "A Multi-dimension end-to-end CNN model for rotating devices fault diagnosis on high-speed train bogie." *IEEE Trans. Veh. Technol.*, 69, 2020, pp.2513-2524.
- [25] Z.L. Liu, H. Wang, J.J. Liu, Y. Qin, and D.D. Peng. "Multitask learning based on lightweight 1DCNN for fault diagnosis of wheelset bearings." *IEEE Trans. Instrum. Meas.*, 70, 2021.
- [26] J.H. Wang, J.W. Yang, Y.Z. Wang, Y.L. Bai, T.L. Zhang, D.C. Yao. "Ensemble decision approach with dislocated time-frequency representation and pre-trained CNN for fault diagnosis of railway vehicle gearboxes under variable conditions." *Int. J. Rail Transp.*, 10, 2022, pp.655-673.
- [27] Y.Y. Zou, Y.D. Zhang, and H.C. Mao. "Fault diagnosis on the bearing of traction motor in high-speed trains based on deep learning." *Alex. Eng. J.*, 60, 2021, pp.1209-1219.
- [28] M.A. Abbasi, S. Huang, and A.S. Khan. "Fault detection and classification of motor bearings under multiple operating conditions." *ISA transactions.*, 2025 Jan 1, 156, 61-9.
- [29] Z. Zhang, N. Li, C. Zang, N. Yuan, and H. Qian, "A novel fault diagnosis based on fft-1dcnn," *7th ICEMCE*, 2023, pp. 692-697.

- [30] J. Cooley and J. Tukey, "An algorithm for the machine calculation of complex fourier series," *Math. Comput.*, 19, 1965, pp. 297–301.
- [31] Y. LeCun and Y. Bengio. "Convolutional networks for images, speech, and time series." The handbook of brain theory and neural networks. 1995 Apr. 3361(10).
- [32] L. Le, A. Patterson, and M. White, "Supervised autoencoders: Improving generalization performance with unsupervised regularizers," *Advances in neural information processing systems*, 31, 2018.
- [33] A.M. Aradhya, A. Ashfahani, F. Angelina, M. Pratama, R.F. de Mello, and S. Sundaram. "Autonomous CNN (AutoCNN): A data-driven approach to network architecture determination." *Information Sciences*, 607, 2022, pp.638-653.
- [34] H.C. Lin, Y.C. Ye, B.J. Huang, and J.L. Su. "Bearing vibration detection and analysis using enhanced fast Fourier transform algorithm." *Advances in mechanical engineering*, 8(10), 2016.